

IMPROVED LATTICE QCD ACTIONS FOR HADRON PHENOMENOLOGY

DEREK B. LEINWEBER

*Department of Physics and Math. Physics, University of Adelaide 5005, Australia
E-mail: dleinweb@physics.adelaide.edu.au*

FRANK X. LEE

*Nuclear Physics Laboratory, Department of Physics, University of Colorado,
Boulder, CO 80309-0446
E-mail: fxlee@sammy.colorado.edu*

The masses and dispersions of light hadrons are calculated in lattice QCD using an $O(a^2)$ tadpole-improved gluon action and the D χ 34 action, an $O(a^2)$ tadpole-improved next-nearest-neighbor fermion action originally proposed by Hamber and Wu. Two lattices of constant volume with lattice spacings of approximately 0.40 fm and 0.24 fm are considered. The results reveal some scaling violations at the coarser lattice spacing on the order of 5%. At the finer lattice spacing, the calculated N/ρ mass ratio reproduces state-of-the-art results using unimproved actions. Good dispersion and rotational invariance up to momenta of $pa \simeq 1$ are also found. The relative merit of alternative choices for improvement operators is assessed through close comparisons with other plaquette-based tadpole-improved actions.

1 Introduction

Lattice discretization of the continuum QCD action introduces errors at finite lattice spacing a . The standard Wilson gauge action has $O(a^2)$ errors and the standard Wilson fermion action has $O(a)$ errors. Simulations using these actions have shown that lattice spacings of 0.1 fm or less and lattice volumes of 24^4 or larger are needed in order to hold systematic errors to the 10% level. Such simulations are major undertakings^{1,2} and require enormous computing power to extract even the most basic of hadronic observables, the hadron masses.

During the past few years, considerable efforts have been devoted to improving lattice actions^{3,4}. The idea is to reduce or remove the discretization errors from the actions so that they have better continuum-like behavior. At the same time, errors due to the lattice regularization are accounted for through the renormalization of the coefficients multiplying the improvement operators. The hope is the use of improved actions will allow one to simulate efficiently

Presented by D.B.L. at the workshop on "Nonperturbative Methods in Quantum Field Theory," CSSM, Adelaide, Feb. 2-13, 1998. This and related papers may be obtained from: <http://www.physics.adelaide.edu.au/theory/staff/leinweber/publications.html>

and accurately on coarse lattices, such that computer resources may be redirected to the simulation of QCD rather than quenched QCD. Moreover, one may turn the focus of investigation towards quantities of experimental interest.

In the pure gauge sector, the $O(a^2)$ tadpole-improved action⁵ leads to dramatic improvement in the static potential and glueball masses⁶ up to lattice spacings of 0.4 fm. In the light quark sector, hadron spectroscopy has been investigated with a variety of improved actions including the $O(a)$ -improved SW action⁷, the $O(a^2)$ -improved D234 action⁸ and its variants^{3,9}, and the D χ 34 action of Hamber and Wu^{10,11,12,13} considered here.

The D χ 34 action is an $O(a^2)$ next-nearest-neighbor fermion action with tadpole-improved estimates of the coupling renormalizations. This action is selected primarily due to its simplicity. The cost of simulating it is about a factor of two as compared to standard Wilson fermions. Our goal is to study its feasibility as an alternative action to SW which has the clover term, or to D234 which has both next-nearest-neighbor couplings and the clover term. In particular, we examine dispersion relations and test the rotational symmetry of both the gauge and the fermion actions. Hadron mass ratios are calculated for a wide variety of hadrons including hyperons. To explore scaling violations, we consider two coarse lattices of approximately fixed physical volume: $6^3 \times 12$ at a lattice spacing of 0.40 fm and $10^3 \times 16$ at 0.24 fm.

2 Improved Lattice Actions

The improved gauge action employed in this investigation is given by⁵:

$$S_G = \beta \sum_{\text{pl}} \frac{1}{3} \text{Re Tr}(1 - U_{\text{pl}}) - \frac{\beta}{20u_0^2} \sum_{\text{rt}} \frac{1}{3} \text{Re Tr}(1 - U_{\text{rt}}). \quad (1)$$

The second term removes the $O(a^2)$ errors at tree level. Perturbative corrections are estimated⁵ to be of the order of 2-3%. Here, U_{rt} denotes the rectangular 1x2 plaquettes. u_0 is the tadpole factor that largely corrects for the large quantum renormalization of the links $U_\mu(x) = \exp(i g \int_x^{x+a\hat{\mu}} A(y) \cdot dy)$. In this calculation we use the mean plaquette $u_0 \equiv (\text{Re Tr}\langle U_{\text{pl}} \rangle)^{1/4}/3$ to estimate u_0 , and will focus our evaluation of lattice action improvement on other plaquette-based improved actions. u_0 is determined self-consistently in the simulation.

The improvement program of Sheikoleslami and Wohlert (SW)¹⁴ provides a systematic approach to the improvement of lattice fermion actions. However, the on-shell improvement program leaves some freedom in the relative values of the coefficients of the improvement operators. In this investigation, we consider

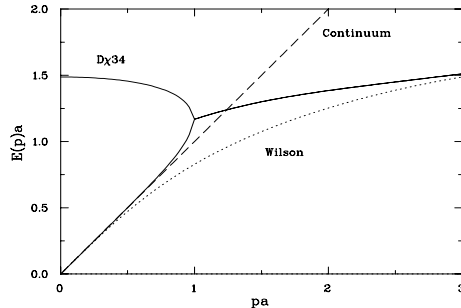


Figure 1: Free dispersion relations for zero mass $D\chi_{34}$, Wilson, and continuum fermions. Momentum p is along the $(1,1,0)$ direction. Beyond the $D\chi_{34}$ branch point, the real part of the two conjugate roots is shown.

a specific case of the general class of D234 actions⁹ in which the improvement parameters are tuned to remove the second-order chiral-symmetry-breaking Wilson term at tree level. This fermion action may be written

$$M_{D\chi_{34}} = m_q + \gamma \cdot \nabla + \frac{1}{6} \sum_{\mu} (-a^2 \nabla_{\mu} \Delta_{\mu} + b a^3 \Delta_{\mu}^2) \quad (2)$$

where

$$\nabla_{\mu} \psi(x) = \frac{1}{2a u_0} [U_{\mu}(x) \psi(x + \mu) - U_{\mu}^{\dagger}(x - \mu) \psi(x - \mu)] , \quad (3)$$

and

$$\Delta_{\mu} \psi(x) = \frac{1}{a^2 u_0} [U_{\mu}(x) \psi(x + \mu) + U_{\mu}^{\dagger}(x - \mu) \psi(x - \mu) - 2 u_0 \psi(x)] . \quad (4)$$

The second-order term of the D234 action, $\sum_{\mu} \Delta_{\mu} + \sigma \cdot F/2$, breaks chiral symmetry and does not appear in the $D\chi_{34}$ action. The fourth-order term of (2) breaks chiral symmetry and provides for the removal of the fermion doublers. The $D\chi_{34}$ action is free of both $O(a)$ and $O(a^2)$ errors at tree level. Explicit evaluation of (2) combined with a Wilson-fermion-style field renormalization, discloses the fermion action of Hamber and Wu^{10,11,13}.

Free dispersion relations can be obtained by locating the poles in the fermion propagator. Fig. 1 shows free dispersion relations for massless continuum, Wilson, and $D\chi_{34}$ fermions. It is clear that $D\chi_{34}$ fermions follow the continuum more closely than Wilson fermions. Note that there exists an unphysical high energy doubler (or ghost) in the $D\chi_{34}$ action. It is very similar to that for the D234 action⁸ and is a general feature of fermions with

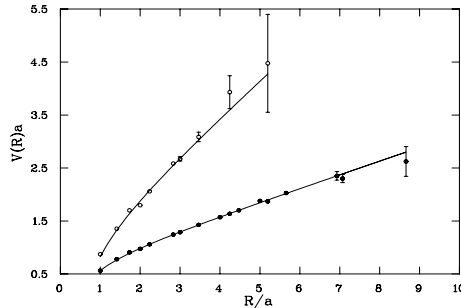


Figure 2: Static potential from Wilson loops. The empty circles are for $\beta = 6.25$, the solid circles for $\beta = 7.0$. The lines are best fits. The statistical errors are from 200 configurations in both cases.

next-nearest-neighbor couplings. The doubler can be ‘pushed away’ from the low momentum region by various techniques, such as tuning the value of b , or using an anisotropic lattice⁹. We simulate with $b = 1$, which gives good dispersion to $pa \sim 1$ as illustrated in Fig. 1.

3 Lattice Simulations

3.1 Methods and Parameters

Quenched gauge configurations are generated using the Cabibbo-Marinari pseudo-heat-bath method¹⁵. Periodic boundary conditions are used in all directions for the gauge field and in spatial directions for the fermion field. Dirichlet boundary conditions are used for the fermion field in the time direction. Configurations separated by 300 sweeps are selected after 4000 thermalization sweeps from a cold start.

The static potential is calculated and the string tension σ is extracted from the ansatz $V(R) = V_0 + \sigma R - E/R$ where V_0 and E are constants. Fig. 2 shows our results. Good rotational invariance of the static potential is observed. Using $\sqrt{\sigma} = 440$ MeV to set the scale, the lattice spacings for the coarse and fine lattices are 0.40(6) fm and 0.23(1) fm with χ^2/N_{DF} of 1.46 and 0.91 respectively. We analyze 155 configurations on our coarse $6^3 \times 12$ lattice and 100 configurations on our fine $10^3 \times 16$ lattice.

Five quark propagators are computed by the Stabilized Biconjugate Gradient algorithm¹⁷ for each configuration. The five quark masses selected are approximately 210, 180, 150, 120, 90 MeV, for both lattices. The second value, 180 MeV, is taken as the strange quark mass. A point source is used at space-time location $(x,y,z,t)=(1,1,1,2)$ on the $6^3 \times 12$ lattice and $(1,1,1,3)$ on the

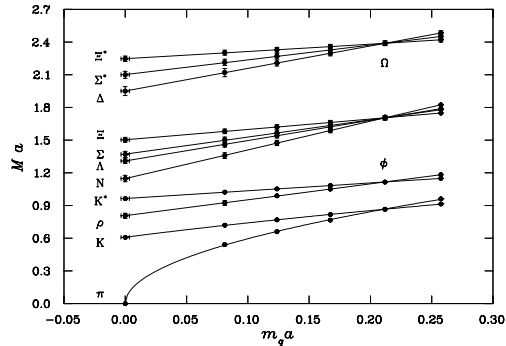


Figure 3: Hadron masses in lattice units as a function of m_q on our fine lattice. The lines are chiral fits as discussed in the text. For better viewing, the decuplet masses are shifted upward by 0.5 unit.

$10^3 \times 16$ lattice. The gauge-invariant smearing method¹⁸ is applied at the sink to increase the overlap of the interpolating operators with the ground states.

Statistical errors are estimated in a third-order, single-elimination jackknife, with bias corrections¹⁹. A third-order jackknife provides uncertainty estimates for the correlation functions, fits to the correlation functions, and quantities extrapolated to the chiral limit.

3.2 Hadron Masses

Fig. 3 shows the extracted hadron masses plotted as a function of the quark mass. We report values taken from covariance matrix fits to the time slice interval 4 through 8 on our coarse lattice and 6 through 9 on our fine lattice. These regimes provide the best signal-to-noise and good correlated χ^2/N_{DF} . κ_{cr} is determined by linearly extrapolating m_π^2 as a function of m_q to zero. Similarly, the pseudoscalar kaon is extrapolated via $m_K^2 = c_0 + c_1 m_q$. The form $M = c_0 + c_1 m_q$ is used for all other extrapolations to the chiral limit. Fits including an additional term $c_2 m_q^{3/2}$ are also considered and similar results are found with slightly larger error bars.

Ratios of the chirally extrapolated masses are given in Table 1 along with the ratios as observed in nature²⁰. At $\beta = 7.0$ the lattice spacing estimates follow the familiar pattern having the value based on the string tension lying between that of the ρ and nucleon based values. This is most likely an artifact of the quenched approximation. However, at $\beta = 6.25$ we find significant disagreement among the values and an unusual reordering of values.

Focusing first on ratios of hadrons having the same angular momentum,

Table 1: Mass ratios after extrapolation to the chiral limit. a_ρ and a_N are lattice spacings in fm set by the rho mass (770 MeV) and the nucleon mass (938 MeV).

	$\beta=6.25$	$\beta=7.0$	Expt.		$\beta=6.25$	$\beta=7.0$	Expt.
Vector/Vector				Pseudoscalar/Vector			
K^*/ρ	1.20(2)	1.20(2)	1.16	K/ρ	0.76(2)	0.75(2)	0.64
ϕ/ρ	1.40(3)	1.39(3)	1.32				
Octet/Octet				Octet/Vector			
Λ/N	1.16(2)	1.16(1)	1.19	N/ρ	1.48(6)	1.44(5)	1.22
Σ/N	1.19(2)	1.20(1)	1.27	Λ/ρ	1.72(6)	1.66(5)	1.45
Ξ/N	1.34(3)	1.33(2)	1.40	Σ/ρ	1.76(6)	1.72(5)	1.55
				Ξ/ρ	1.97(6)	1.91(6)	1.71
Decuplet/Decuplet				Decuplet/Vector			
Σ^*/Δ	1.12(1)	1.11(1)	1.12	Δ/ρ	1.79(7)	1.77(5)	1.60
Ξ^*/Δ	1.24(3)	1.22(2)	1.24	Σ^*/ρ	2.00(6)	1.97(6)	1.80
Ω/Δ	1.34(3)	1.33(2)	1.36	Ξ^*/ρ	2.20(7)	2.16(6)	1.99
				Ω/ρ	2.40(7)	2.35(6)	2.17
String Tensions				Decuplet/Octet			
a_{st}	0.40(3)	0.220(2)		Δ/N	1.21(5)	1.23(2)	1.31
a_ρ	0.30(1)	0.205(6)		Σ^*/N	1.35(5)	1.37(2)	1.47
a_N	0.36(1)	0.242(6)		Ξ^*/N	1.49(4)	1.50(3)	1.63
				Ω/N	1.63(4)	1.64(3)	1.78

we see very little change in the values as the lattice spacing is decreased. These ratios are also remarkably similar to those observed in nature, despite the fact that these are quenched QCD calculations. In addition, these ratios support our selection for the strange quark mass.

This close resemblance to nature is not shared by ratios of hadrons with different angular momentum. All four classes of ratios significantly disagree with those of nature. Once again we see the familiar quenched artifact of the Octet/Vector ratio being too large and the Decuplet/Octet ratio being too small.

The standard failure of the K/ρ mass ratio in the quenched approximation is also seen here. This shortcoming has been widely realized through an examination of the J -parameter²¹ defined by

$$J = m_\rho \left. \frac{dm_\rho}{dm_\pi^2} \right|_{m_\rho/m_\pi=1.8} \simeq m_{K^*} \frac{m_{K^*} - m_\rho}{m_K^2 - m_\pi^2}. \quad (5)$$

Empirically this ratio is 0.48. However we find 0.42 on our coarse lattice and 0.43 on our fine lattice. The physics associated with this discrepancy was

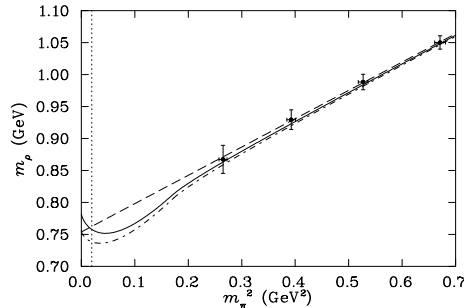


Figure 4: Plot of the ρ -meson mass as a function of the squared pion mass obtained from our finer lattice. a_ρ has been used to set the scale. The dashed line illustrates the standard linear extrapolations of m_π^2 and m_ρ . The solid and dot-dash curves include the two-pion self-energy of the ρ meson²² for dipole dispersion cut-off values of 1 and 2 GeV respectively. The increase in the slope at $m_\rho/m_\pi = 1.8$ ($m_\pi^2 \simeq 0.21$) provided by the two-pion self energy is the right order of magnitude to restore agreement with the empirical value.

first reported by Cohen and leinweber²² where it was pointed out that the self-energy generated by two-pion intermediate states of the ρ -meson, which is excluded in the quenched approximation, acts to increase the J parameter. Fig. 4 provides a sketch of how including the two-pion self-energy of the ρ can increase the value of J to 0.46.

Perhaps the most important information displayed in Table 1 is that the Octet/Vector mass ratios display less than satisfactory scaling for the larger lattice spacing. To further examine scaling and make contact with other studies, we focus on the the N/ρ mass ratio which is among the the most revealing of ratios.

Fig. 5 shows a comparison of the N/ρ mass ratio versus $M_\rho a$ at the chiral limit. Fig. 6 shows the N/ρ mass ratio as a function of $M_\rho a$ at a fixed π/ρ mass ratio²⁴ of 0.7. This method is free of complications from chiral extrapolations. Both cases clearly show the improvement provided by the D χ 34 action. Indeed, the D χ 34 action has reproduced the state-of-the-art quenched QCD ratios using unimproved actions at coarse lattice spacings of 0.24 fm.

3.3 Dispersion and Rotational Symmetry

In addition to mass ratios, hadron states at finite momentum projections $\vec{p}a = \vec{n}(2\pi/L)$ are also calculated. Dispersion is examined by calculating the effective speed of light, defined by $c^2 = (E^2(p) - E^2(0))/p^2$, which is to be compared with 1.

A comparison with SW and D234 lattice actions⁸ is made in Table 2.

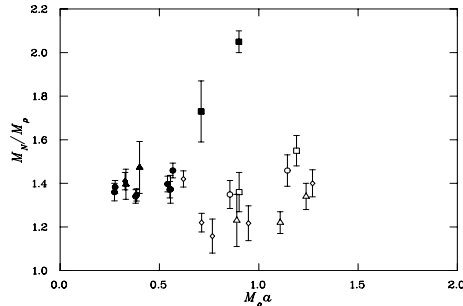


Figure 5: The N/ρ mass ratio versus $M_\rho a$ at the chiral limit. Solid symbols denote the standard Wilson action. Open symbols denote improved actions including SW⁷ (\diamond), D234⁸ (\triangle), $D\chi_{34}$ ¹² (\square), and $D\chi_{34}$ (\circ) (this work).

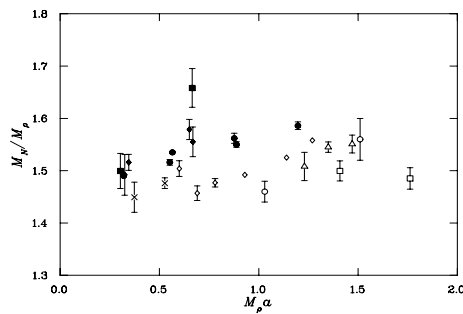


Figure 6: The N/ρ mass ratio versus $M_\rho a$ at a fixed π/ρ mass ratio of 0.7 for various actions. The solid symbols denote the standard actions: Wilson (square and diamond), staggered (circle). The open symbols denote improved actions: nonperturbatively-improved SW²³ (\times), fixed-point action²⁴ (\square), SW (\diamond), D234 (\triangle), and $D\chi_{34}$ (\circ) (this work).

The dispersion for the $O(a)$ -improved SW action is very poor relative to the excellent dispersions of the next-nearest-neighbor improved Dx_{34} actions in general. The $D\chi_{34}$ dispersion is excellent even at our coarse lattice spacing.

Rotational symmetry is explored in Table 3. At the coarser lattice spacing, some drift in the central values is seen for the pion and nucleon. The drift in the pion is similar to that seen for the D234c action³. However, the drift in dispersion previously reported for the ϕ meson³ is not apparent in our results for the $D\chi_{34}$ action. The $D\chi_{34}$ action has much better rotational symmetry than the SW action³. The $D\chi_{34}$ action provides satisfactory dispersion at our finer lattice spacing and is competitive with the D234 action⁸.

Table 2: Comparison of SW, D234 and D χ 34 actions for the speed of light squared obtained from the dispersion of π and ρ mesons at $m_\pi/m_\rho \simeq 0.7$ for $pa = (2\pi/L)$.

Hadron	a (fm)	SW	D234	D χ 34
π	0.40	0.63(2)	0.95(2)	0.99(3)
π	0.24		0.99(4)	1.04(4)
ρ	0.40	0.48(4)	0.93(3)	0.93(6)
ρ	0.24		1.00(6)	0.99(6)

Table 3: Evaluation of dispersion and rotational invariance via the effective speed of light. The results are for $m_q \sim 180$ MeV.

a (fm)	\vec{n}	π	ϕ	N	Ω
0.40	(1,0,0)	0.98(2)	0.91(4)	1.00(7)	0.99(12)
	(1,1,0)	0.91(4)	0.91(6)	0.94(8)	0.91(7)
	(1,1,1)	0.86(9)	0.92(10)	0.92(7)	0.90(10)
0.24	(1,0,0)	1.04(3)	1.02(4)	1.10(6)	1.06(7)
	(1,1,0)	1.05(4)	1.02(4)	1.06(5)	1.11(5)
	(1,1,1)	0.98(6)	0.98(6)	1.06(6)	1.06(5)

4 Conclusion

We have computed masses and dispersion relations of light hadrons in lattice QCD using tree-level $O(a^2)$ tadpole-improved gauge and fermion actions. These actions have the appeal of being simple to implement and inexpensive to simulate. A great deal of effort is being directed toward finding the ultimate improved action that will facilitate simulations on the coarsest of lattices. We note however, that many quantities of phenomenological interest such as hadron form factors involve momenta on the order of a GeV. As such, a highly improved action which is costly to simulate may not be the ideal action for hadron phenomenology, especially for exploratory purposes.

The mass ratios obtained from the D χ 34 action at 0.24 fm on a modest $10^3 \times 16$ lattice reproduce the state-of-the-art results using conventional unimproved actions. Excellent dispersion and rotational invariance up to $pa \approx 1$ are also found. These results demonstrate that the D χ 34 action can serve as a viable candidate for the study of hadron phenomenology, and in our view is

preferable to the highly-improved but more costly D234 action. We plan to use the $D\chi_{34}$ action to study hadron properties beyond the spectrum, such as multipole form factors of hadrons in general. These results also bode well for future explorations beyond the quenched approximation.

Support from the U.S. DOE and the Australian Research Council is gratefully acknowledged.

References

1. Butler et al., Nucl. Phys. **B 430**, 179 (1994).
2. T. Yoshié, hep-lat/9711017.
3. P. Lepage, hep-lat/9707026.
4. P. Hasenfratz, hep-lat/9709110.
5. M. Alford, W. Dimm, P. Lepage, Phys. Lett. **B361**, 87 (1995).
6. C. Morningstar and M. Peardon, hep-lat/9704011.
7. S. Collins, R.G. Edwards, U.M. Heller, and J. Sloan, Nucl. Phys. (Proc. Suppl.) **B47**, 366 (1997), Nucl. Phys. (Proc. Suppl.) **B53**, 206 (1997), Nucl. Phys. (Proc. Suppl.) **B53**, 877 (1997),
8. M. Alford, T. Klassen and P. Lepage, Nucl.Phys. (Proc. Suppl.) **B47**, 370 (1996), hep-lat/9509087.
9. M. Alford, T. Klassen and P. Lepage, hep-lat/9608113, hep-lat/9611010, hep-lat/9709126.
10. H. Hamber and C.M. Wu, Phys. Lett. **B133**, 351 (1983); **B136**, 255 (1984).
11. T. Eguchi and N. Kawamoto, Nucl. Phys. **B237**, 609 (1984).
12. H.R. Fiebig and R.M. Woloshyn, Phys. Lett. **B385**, 273 (1996).
13. F.X. Lee and D.B. Leinweber, U. Adelaide PP ADP-97-44/T272. U. Colorado PP CU-NPL-1154, hep-lat/9711044.
14. B. Sheikoleslami and R. Wohlert, Nucl. Phys. **B259** (1985) 609.
15. N. Cabibbo and E. Marinari, Phys. Lett. **B 119**, 387 (1982).
16. R. Sommer, Nucl. Phys. **B411**, 839 (1994).
17. A. Frommer, *et al.*, hep-lat/9404013.
18. S. Güsken, Nucl.Phys. (Proc. Suppl.) **B17**, 361 (1990).
19. B. Efron, SIAM Rev. **21**, 460 (1979); S. Gottlieb, P.B. MacKenzie, H.B. Thacker, and D. Weingarten, Nucl. Phys. **B 263**, 704 (1986).
20. Particle Data Group, Phys. Rev. D **50**, (1994).
21. P. Lacock and C. Michael, Phys. Rev. **D52**, 5213 (1995).
22. D.B. Leinweber and T. Cohen, Phys. Rev. **D49**, 3512 (1994).
23. M. Göckeler, et. al., hep-lat/9707021.
24. T. DeGrand, hep-lat/9709052, and private communication.